Optimal Antenna Locations for Coverage Extension in Sub-Terahertz Vehicle-to-Vehicle Communications

Dmitri Moltchanov, Vitalii Beschastnyi, Darya Ostrikova, Yuliya Gaidamaka,
Yevgeni Koucheryavy, and Konstantin Samouylov

***Abstract*—Sub-terahertz (sub-THz, $100-300$ GHz) communications promise to bring extraordinary rates in future 6G systems. High path loss and blockage effects will limit the coverage of base stations (BS) to a few hundred meters making deployment of such systems along the roads expensive. As a way to decrease the BS density, relaying has been proposed. However, vehicle-to-vehicle (V2V) propagation is characterized by different sets of communications paths depending on the antenna locations raising the question of their optimal positions. In this paper, by utilizing IEEE 802.15.3d parameters and 300 GHz propagation measurements, we develop a mathematical framework for comparison of multi-hop relaying systems with different antenna locations. We utilize coverage, BS availability, and the data rate over a multi-hop path as metrics of interest. Our results show that the windshield location is characterized by lower data rates and larger coverage while bumper and engine levels are similar in terms of these metrics. For the windshield location, the coverage is extended by 50% with BS availability 0.95. The windshield location is recommended as it is less sensitive to the technology penetration rate and is characterized by larger coverage. The proposed approach shows gains of up to 32% in terms of required BS density for the range of vehicles density (10-40 units/km).**

I. Introduction

5G New Radio (NR) systems operating in the microwave (μWave) and millimeter wave (mmWave) bands already hit the market. At the same time, the researchers have already started to investigate even higher sub-terahertz (sub-THz, $100-300$ GHz) bands in the context of 6G systems [1], [2]. However, extremely high propagation losses, dynamic blockage effects [3], [4] as well as micromobility [5]–[7] will limit the coverage range of such systems to just a few hundred meters.

One of the biggest challenges for network operators is to enable enhanced mobile broadband service (eMBB) for users inside moving vehicles. This service requires not only permanent connectivity but high access rates [8]. To enable it, high capacity 5G NR operating in mmWave band or 6G sub-THz systems can be utilized. However, the inherently high path losses in the sub-THz band, as well as other propagation phenomena such as blockage limit the coverage of base stations (BS) located on the roadside to a few hundred meters or even less requiring dense cost-inefficient deployments.

Propagation conditions in vehicle-to-vehicle (V2V) communications drastically differ from those in conventional cellular deployments. To this aim, several large-scale simulation campaigns in both mmWave and sub-THz bands have been performed recently as discussed in detail in Section II. Their results indicate that (i) there are multiple potential propagation paths between communicating entities on the road and (ii) the set of the available propagation path may drastically differ depending on the location of antennas. These observations have also been confirmed by the results of link-level performance evaluation studies performed so far, see Section II for a detailed review.

To ensure permanent connectivity and reduce capital expenditures of network operators, relaying functionality can be utilized [9]. To provide this support, 3GPP recently standardized integrated access and backhaul (IAB) technology [10], [11] with plans to extend it to mobile IAB nodes in Release 18. 3GPP also initiated work on NR-sidelink technology allowing for the establishment of device-to-device (D2D) links [12], [13]. By relying upon these technological enablers, vehicles along the road equipped with appropriate sub-THz high-speed interfaces may organize the so-called multi-hop "bridges" by forwarding data of vehicles that currently do not have direct connectivity with infrastructure. However, the efficiency of this approach heavily depends on two critical metrics of these bridges, data rate, and length, which are in their turn influenced by the locations of antennas. To the best of the authors' knowledge, the question of optimal locations of antennas ensuring the minimal possible deployment density of BS has not been addressed in the literature.

The ultimate aim of our study is to identify the optimal location of antennas resulting in the minimal density of infrastructure BSs for a given set of deployment parameters and road traffic conditions. Simultaneously, we also require that certain metrics of interest for vehicles utilizing the relaying service are to be satisfied, i.e., we report minimal BS density ensuring that connectivity of vehicles is satisfied with a prescribed probability. The developed analytical framework relies upon recent measurements of sub-THz propagation in V2V environment and utilizes realistic sub-THz communications parameters from IEEE 802.15.3d standard. It is built by utilizing the two-step approach: (i) single-hop data rate and communications distance assessment and (ii) characterization

The work in this paper has been supported by the Academy of Finland under the project HARMONIOUS (Machine learning methods and algorithms for 6G terahertz cellular access).

D. Moltchanov and Y. Koucheryavy are with Tampere University, Tampere, Finland. Email: {dmitri.moltchanov, evgeni.kucheryavy}@tuni.fi

D. Ostrikova, V. Beschastnyi, Y. Gaidamaka, K. Samouylov are independent authors. Email: {vabeschastny, d.ostrikova, yuliya.gaidamaka, ksamuylov}@gmail.com

of data rate and inter-site distance (ISD) between BSs ensuring a certain coverage probability. We report our results as a function of deployment, environment, and road traffic conditions.

The main contributions of our study are:

- the mathematical framework for assessment of the minimal required density of roadside THz BSs ensuring connectivity and data rate for vehicles connected over a multi-hop bridge;
- numerical results based on IEEE 802.15.3d parameters and real measurements at 300 GHz illustrating the effect of road traffic and environmental conditions on the multi-hop bridge length and its data rate;
- observations showing that: (i) the windshield antenna location is better than bumper/engine level locations in terms of coverage but is characterized by a lower data rate, (ii) with 70% of technology penetration rate BS availability for windshield antenna location is as high as 0.95 for up to 50% extended BS coverage, (iii) traffic jam conditions are the worst scenario leading to a 10% improvement in coverage, however, as road traffic conditions become sparse it linearly increases.
- recommendation that for initial V2V deployments in sub-THz bands windshield location is to be utilized as it is less sensitive to technology penetration rate and is characterized by larger coverage.

The rest of the paper is organized as follows. First, in Section II we review related work. The system model is introduced in Section III. In Section IV, we develop our performance evaluation framework. Numerical results are presented in Section V. Conclusions are drawn in the final section.

II. Related Work

In this section, we present the related work. We start by reviewing the propagation measurement results for both mmWave and sub-THz bands. Then, we proceed with discussing models and use cases considered in recent literature.

A. Sub-THz and mmWave Propagation in V2V

1) mmWave V2V Measurements: Most of the propagation measurements performed so far in the V2V environment concentrated on the mmWave band. For line-of-sight (LoS) blockage, [14] reports 5–30 dB excess blockage loss for 60 GHz, which depends on the blocker size and the number of intermediate vehicles. The authors in [15] carried out measurements at 30, 60, and 73 GHz showing that the induced blockage is between 5.5 and 17 dB.

To the best of the authors' knowledge, experiments involving different heights of a transmitter (Tx) and receiver (Rx) in the mmWave band are scarce. However, one may refer to the results provided in [15]–[17] reporting that the measured blockage loss at Tx/Rx height of 0.6, 1.5, and 1.7 m (all at 28 GHz). The reported losses are 30-40, 13.3, and 11-12.2 dB, respectively. Note that in [16], [17] different locations of Tx and Rx around the vehicle are considered.

Several studies performed at mmWave frequencies report path loss exponent. Following [14] it is on the order of 0.4–1.8 for 60 GHz, while [18] reports it to be in the range of 1.7–2.2 generally coinciding with the values recommended by 3GPP in [19]. Note that at 60 GHz path loss results might be biased due to the presence of atmospheric absorption. In [20], V2V channel measurements were conducted at 73 GHz in an urban area and the mean path loss exponent is reported to be 2.7.

TABLE I: Measured propagation properties at 300 GHz [21]

Setup	Model
	Single-lane scenarios
LoS propagation	FSPL
Vehicle-body block.	FSPL + height-dependent penetration loss of 30 dB to 50 dB. *Important to account for in the analysis*
Under-vehicle prop.	FSPL + $\phi d^{-\Psi}$, where ϕ and Ψ are as in Table I in [21]. *Important to account for in the analysis*
Front/rear reflection	FSPL + reflection loss of $\sim$25 dB. *May be neglected in first-order studies*
	Multi-lane scenarios
Sym. side reflection	Two-ray model approximation: FSPL + reflection loss of $\sim$3 dB. *Important to account for in the analysis*
Assym. side reflection	Two-ray model approximation: FSPL + angle-dependent loss of 16 dB to 20 dB
Front reflection	Two-ray model approximation: FSPL + angle-dependent loss of 24 dB to 42 dB
Rear reflection	Two-ray model approximation: FSPL + angle-dependent loss of 15 dB to 30 dB

Most of the studies performed so far in the mmWave band mainly concentrated on the abovementioned characteristics while directional characterization of the mmWave V2V channel is generally missing, which significantly limits the application of channel models. To the best of the authors' knowledge, there are no measurement campaigns at mmWave frequencies trying to characterize multi-lane reflections. Similarly, there are no results for single/multi-lane front/rear reflection.

Recently studies characterizing RMS and angular delay spread (DS) of the channel in outdoor environments at THz frequencies started to appear, see e.g., [15], [17], [22]. In all these studies the measurement campaigns have been carried out in outdoor environments at 28, 60, and 73 GHz frequencies. The common conclusion is that the presence of a blocker increases the DS of the channel. Particularly, [17] reports the increase of DS from 2.55 to 4.40 ns (by 56%) and angular DS from 7.87 to 10.53° (by 74%). The data in [15] show the increase of DS from 19 to 44 ns (by 43%) and angular DS from 27.3° to 41.6° (by 65%).

2) Sub-THz Measurements: So far only a limited number of studies reported THz and sub-THz measurements. Specifically, the authors in [23] performed blockage measurements in a V2V propagation environment at 300 GHz for various antenna heights. They reported that depending on the height of Tx and Rx antennas the blockage attenuation varies in the range of $15-40$ dB. In [21], they extended their study to capture exhaustive communications scenarios that may potentially occur in the V2V environment including under-vehicle propagation, traversal through the windshield, multi-lane reflections, front/rear reflections, all at different heights corresponding to bumper, engine, and windshield. As this the is most complete measurement campaign, we utilize it in our study. The relevant data are summarized in Table I.

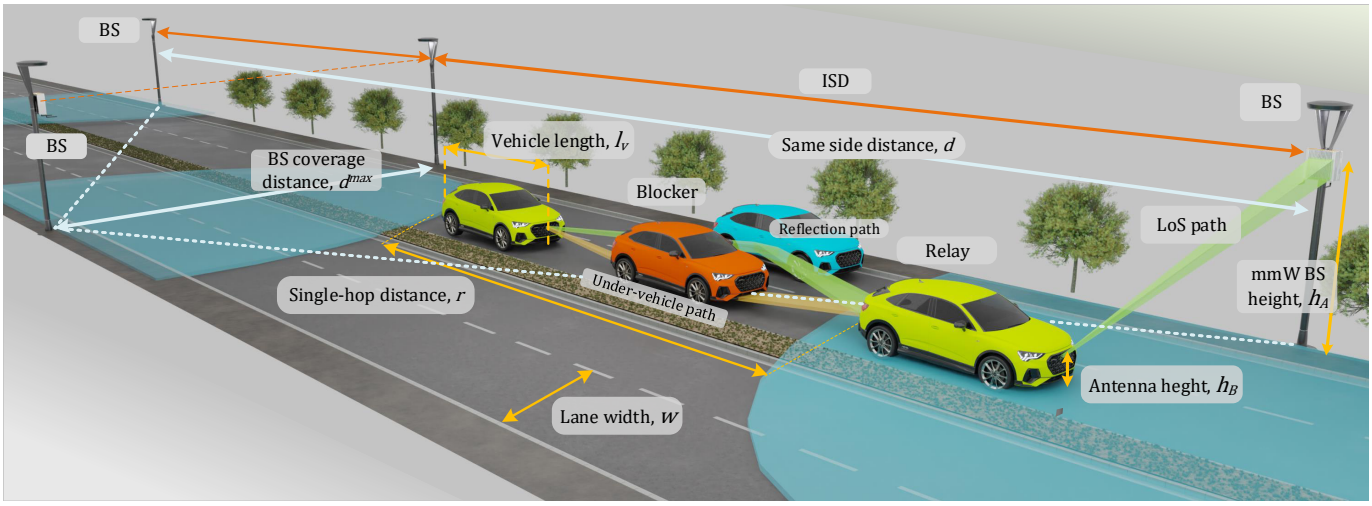

Fig. 1: The considered scenario and main components of the system model.

B. Relay Use-Cases and Deployments

Coverage in V2V deployments has been addressed in many studies so far. Specifically, the authors in [16] studied the influence of antenna location on blockage probability. Six types of antenna locations were analyzed, and it has been shown that the closer the Tx and Rx are located, the more likely the signal is blocked by the car body. The recommended location for the antenna is the side pillars. However, only 10 m and 100 m separation distances between the Tx and the Rx have been addressed. The authors of [24] considered the dependence of the coverage area on signal attenuation. Their results showed that for reliable connectivity the nearest vehicle should be utilized for communications. However, the authors did not consider feasible reflections off vehicles in the adjacent lanes or road as potential communications paths.

A number of studies addressed the problem of interference in V2V deployments. The authors in [25] proposed an analytical model accounting for multiple interference paths including reflections off the cars on side lanes. The main observation of their study was that directional antennas allow to efficiently suppress interference. The work in [26] studied the effect of interference from several vehicles communicating with a BS on the two-lane road. The metrics of interest were the packet loss probability and the average throughput when the signal is blocked by a neighboring vehicle. Their results showed that the packet loss probability mainly depends on the number of antennas installed on the BS.

The authors in [27] considered an urban cross-road scenario. Data transmission between Tx and Rx is organized by relaying the signal from neighboring vehicles that support V2V transmission. The authors focused on algorithms for choosing the next relay by analyzing three well-known schemes and also offering their method for relay selection. The result shown by the proposed relay selection scheme is superior to other methods in terms of packet transmission delay. However, their study does not take into account the blockages caused by other vehicles. In [28], the mmWave relay network with nodes using maximal ratio combining (MRC) and selection combining (SC) types of receivers is analyzed. The authors utilized practical measurements of the propagation conditions and considered signal-to-interference-plus-noise ratio (SINR), spectral efficiency, and blockage probability as the metrics of interest. The results of the study showed that the SC receiver provides better performance in terms of packet losses in most scenarios as compared to the MRC receiver. The work in [29] considers the directional beamforming from several BSs while vehicles move along the road. Each BS has several antenna arrays to cover its road area. The proposed link selection policy was shown to outperform the standard approach by 30%.

C. Summary

Summarizing the related work we emphasize that the problem of selecting the optimal antenna locations on communicating vehicles received only a little attention so far. Furthermore, in spite of the detailed measurements campaign in the V2V environment carried out so far, most of the studies rely on theoretical propagation models that neglect important propagation paths available in V2V deployments such as those under vehicles, reflections off vehicles on neighboring lanes, and through the windshield. In our paper, we will fill this void by utilizing exhaustive measurements in [21] to characterize relying properties on V2V deployments and identify optimal antenna locations maximizing coverage and data rate.

III. System Model

In this section, we introduce our system model. We start by introducing deployment and communications scenarios and then proceed with propagation and antenna models. Finally, we specify the metrics of interest. The notation utilized in this paper is summarized in Table II.

A. Deployment and Environment

We consider a street/road deployment of 6G BSs operating in the sub-THz band as illustrated in Fig. 1. In the considered conditions, BSs are assumed to be installed on both sides of the street, e.g., on lampposts at constant height h_A. The distance between BSs along the same side is d, and they are positioned

TABLE II: Notations

Notation	Description
Deployment Parameters	
λ	Vehicle density on a lane, unit/m
h_B	Antenna deployment height, m
h_A	mmW BS height, m
h_c	Road clearance, m
d	Distance between BS along the same side, m
d_s	Minimum separation distance between vehicles, m
v	Vehicle speed, m/s
l_v	Length of vehicle, m
N_l	Number of lanes
w	Lane width, m
w_v	Vehicle half-width, m
P_E	Technology penetration rate
ζ	Type of a path (L, U, R, W)
σ	Antenna location (B, E, W)
Radio Parameters	
$L_A(f,r)$	Absorption loss, dB
P_T, P_{T_W}	BS emitted power, dB/W
G_A, G_U	Antenna array gain, dBi
γ	Path loss exponent
N_0	Thermal noise, dBi
α	Array HPBW, $^\circ$
θ_m	Array maximum, $^\circ$
$\theta^{\pm}_{3dB}$	Upper and lower 3-dB points, $^\circ$
S	Received signal power, dB
S^{min}	Minimum required Rx sensitivity, dB
f_c	Operational frequency, GHz
ϕ, ψ	Propagation constants
I	Interference, dB
L_A, L_B	Absorption and propagation losses, dB
N_C	Number of MCSs
ω_i	Spectral efficiency of i-th MCS
Intermediate Metrics	
$d_{(\cdot)}(S)$	Achievable distance for considered path (L, U, R, W), m
$d^{max}_{(\cdot)}$	Maximum distance for considered path (L, U, R, W), m
d_O	Distance to the next vehicle, m
r	Single hop distance, m
Δ_α	Shift at available beamwidth, m
f_i	PDF of distances to the i-th neighbor in PPP
f_B	PDF of the distance to bypass a blocker
δ_R	Probability of non-blocked side reflection
δ_U	Minimum distance between a blocker and antenna, m
$f_{H,\sigma}(r)$	Probability of single-hop communication at the distance r
$q_{\zeta,i}$	Probability of using MCS i in a hop of type ζ
$\rho_{\sigma,n}$	Mean rate within active communication on n-hop bridge
Final Metrics	
$p_{C,\sigma}(n,r)$	n-hop bridge availability at distance r
$p_S(r)$	Bridge availability at distance r
$P_{\zeta,\sigma}$	ζ-path usage probability for σ antenna location
$\rho_{S,\sigma}$	Mean bridge rate for σ antenna location, bit/s

on different sides, organizing isosceles triangles, i.e., shifted by half the distance of d between the two consecutive BSs. These BSs serve as Internet access points for users that are located in vehicles.

A road is assumed to have N_l lanes, where N_l is even. The direction of movement of "upper" and "lower" $N_l/2$ lanes is the opposite. The width of each lane is constant and equal to w. The speed of vehicles is assumed to be v. The centers of vehicles organize a Poisson process with an intensity λ. These parameters are utilized in Section V to define several typical road traffic conditions. We further assume that vehicles are of the same constant length l_v, while the road clearance is h_C. The road traffic is assumed to be homogeneous on each lane, i.e. v, λ, and l_v are independent of the considered lane.

By following [24], the emerging V2V technologies will enable effective and secure control over vehicle mobility at the minimum allowed separation distance between any two vehicles $d_s = t_s v$, where v is the vehicles' speed and $t_s = 0.5$ s is the minimum required time for automatic control systems to assess real-time traffic conditions and take preventive actions.

B. Relaying, Connectivity, and Antenna Locations

To reduce capital expenditures, associated with full road coverage by decreasing the inter-BS distance, we assume that a fraction of vehicles P_E is equipped with relaying capabilities. The parameter P_E is referred to as the "technology penetration rate". Vehicles are equipped with two transceivers, one in front and one on the back of the vehicles as shown in Fig. 1. The transceivers are assumed to be connected with high-speed internal bus. We assume that the data rate provided by the bus is sufficient for handling relayed traffic which is confirmed by recent developments [30].

The vehicles equipped with communications capabilities are assumed to require eMBB service provided via BS. If the direct connection is not feasible due to a vehicle being out of the coverage of the nearest BS, we assume that they attempt to utilize relaying capabilities to form the so-called multi-hop bridge consisting of one or more hops. The length of this bridge and its data rate heavily depends on deployment, environmental characteristics, and antenna locations.

We consider the following potential antenna location:

- bumper (B) level: 0.3-0.4 m;
- engine (E) level: 0.4-1.0 m;
- windshield (W) level: 1.0-1.5 m.

We use σ to denote antenna locations, i.e., $\sigma \in \{B, E, W\}$. The locations of antennas not only affect propagation conditions but also the set of available communications paths. For each considered location a number of single-hop transmissions are possible, as discussed further in Section IV. Furthermore, for given environmental characteristics these transmission options may or may not be available. These options are characterized by different link lengths and thus data rates.

C. Propagation Model

The value of SINR at the UE at the distance x from the BS is written as [31]

$$S(x) = P_T G_A G_U \Big[\frac{x^{-\gamma}}{(N_0 + I) L_A(f,x) L_B} \Big], \tag{1}$$

where γ is the path loss exponent, I is the interference, N_0 is the thermal noise, P_T is emitted power, G_A and G_U are the transmit and receive side gains, $L_A(f,x)$ is the absorption losses, L_B represents impairments caused by blockage or reflections.

We account for absorption losses by utilizing the results of [31], [32]. More specifically, the absorption loss is defined as

$$L_A(f,x) = \frac{1}{\tau(f,x)}, \tag{2}$$

where $\tau(f,x)$ is the transmittance of the medium following the Beer-Lambert law, $\tau(f,x) \approx e^{-K(f)x}$, $K(f)$ is the overall absorption coefficient of the medium.

The frequency-dependent absorption coefficient $K(f)$ can be represented as [32]

$$K(f) = \sum_{i,g} k^{i,g}(f), \tag{3}$$

where $k^{i,g}(f)$ represents the individual absorption coefficient for the isotopologue i of gas g. We utilize the standard air having 78.1% of nitrogen and 20.9% of oxygen, at the standard altitude with a water vapor fraction of 2%. The coefficients $k^{i,g}$ are available from the HITRAN database [33].

For practical calculation of the absorption coefficient, we utilize the worst-case approximation, $K = \max_f K(f)$ leading to the SINR in the following form

$$S(x) = P_T G_A G_U \Big[\frac{x^{-\gamma} e^{-Kx}}{(N_0 + I) L_B}\Big]. \tag{4}$$

The utilized values of propagation exponent can be deduced from the literature reviewed in Section II. Specifically, for the sub-THz band, by following [21] we utilize $\gamma = 2.0$. Finally, the last remaining term in the denominator of (4) is L_B capturing the effect of the additional impairment. This term heavily depends on the considered communications scenario and can represent either blockage losses induced by propagation through windshields or attenuation caused by reflections off road surface or vehicle body as discussed further in Section IV. We capture the interference in 4 by utilizing the interference margin computed according to [25].

D. Antenna Model

We assume planar antenna arrays at both the BS and the UE. Similarly to [34], [35], we utilize a cone model with the beamwidths corresponding to the half-power beamwidth (HPBW) of the antenna radiation pattern. Using [36], the mean antenna gain over HPBW is

$$G = \frac{1}{\theta^{+}_{3db} - \theta^{-}_{3db}} \int_{\theta^{-}_{3db}}^{\theta^{+}_{3db}} \frac{\sin(N_{(\cdot)}\pi\cos(\theta)/2)}{\sin(\pi\cos(\theta)/2)} d\theta, \tag{5}$$

where $N_{(\cdot)}$ is the number of antenna elements in the appropriate plane. The HPBW of the array, α, can be determined as $\alpha = 2|\theta_m - \theta^{\pm}_{3db}|$, where θ_m is the array maximum that can be computed as $\theta_m = \arccos(-1/\pi)$, $\theta^{\pm}_{3db}$ are the upper and lower 3dB points estimated as $\theta^{\pm}_{3db} = \arccos[\pm 2.782/(N_{(\cdot)}\pi)]$.

The antenna is 3D one with a conical representation of the main lobe similar to the one utilized in [37], [38]. For each plane, we utilize (5) to determine these parameters. For practical calculations, we employ HPBW approximation given by $102^{\circ}/N_{(\cdot)}$ [36], [39]. Similarly, the linear gain can be approximated by the number of elements [36].

E. Metrics of Interest and Approach

The ultimate aim of our study is to identify the location of antennas resulting in the minimal density of infrastructure BSs for a given set of deployment parameters and road traffic conditions. We consider two such metrics: (i) connectivity metric expressed as bridge availability and (ii) rate provided over multi-hop bridge. Specifically, the sought density has to ensure the coverage probability is not lower than certain values, e.g., 0.95.

TABLE III: Utilized modulation and coding schemes

MCS ID	Modulation	Receiver sensitivity (dBm)	Data rate (Gb/s)
0	BPSK	-67	1,29
2	QPSK	-64	2,58
3	QPSK	-60	3,29
4	8-PSK	-59	3,87
8	16-QAM	-57	5,16
9	16-QAM	-53	6,57
10	64-QAM	-52	7,74
11	64-QAM	-47	9,86

By introducing multi-hop cellular communications in the IAB architecture, 3GPP has not relaxed any requirements on the metrics of interest achieved data rates over the air interface for 5G [8]. Thus, achieving high data rates remains one of the crucial metrics in IMT-2020/2030 systems [40], [41]. The bridge availability metric stems from the quality of service requirements of network operators that need to dimension their systems such that only a tiny fraction of UEs at the edge are in outage conditions, e.g., this metric is often chosen from the range 1% – 5% [42]. In addition to these two metrics, a critical measure of QoS for multi-hop cellular communications is the latency as traversal of each hop adds queuing delay and additional impairments related to, e.g. half-duplex communications in different antennas [11]. We do not study this metric explicitly, instead considering the bridge availability and attained rate metrics as a function of the number of hops.

In what follows, we take a two-staged approach. In the first stage, in Section IV, we characterize single-hop characteristics including the data rate and communications distance for all considered antenna locations. Then, we utilize these metrics to assess the bridge length under connectivity and data rate constraints. Finally, we utilize the latter results to express the density of roadside BS deployment under given road traffic and environmental conditions.

IV. Performance Evaluation Framework

In this section, we develop our performance evaluation framework. We start with the single-hop characterization of communications distances and attained rate over feasible propagation paths. Then, we proceed to formalize multi-hop communications scenario. Finally, we specify the metrics of interest.

A. Single-Hop Path Length and Data Rate

We start with single-hop communications distances and data rates. To derive them, we utilize the set of modulation and coding schemes specified in IEEE 802.15.3d standard [43], see Table III and measurements of the propagation paths in the V2V environment reported in [21] and provided in Table I.

By following the propagation measurements in [21], the maximum communication distance with tolerable received signal power S for LoS conditions is written as

$$d_L(S) = \left(\frac{P_T \sqrt[10]{10^{G_A + G_U}}}{\sqrt[10]{10^{N_0 + S}} 10^{2log_{10} f_c - 14,86}} \right)^{\frac{1}{\gamma}}, \tag{6}$$

where P_T is the transmit power, G_A and G_U are the transmit and receive side gains, f_c is the carrier frequency, and N_0 is the thermal noise.

For all the considered antenna locations, the LoS path is available as long as the next vehicle supports multi-hop relaying and the distance is smaller than a certain maximum $d^{\max}$. When the neighbor vehicle does not support multi-hop relaying, for bumper antenna location level, in addition to LoS path (L), under-vehicle (U) and side refection (R) propagation paths might be available. For engine and windshield antenna locations the under-vehicle propagation path is not available due to geometrical restrictions. The rationale is that we do not consider non-peculiar reflections off the vehicles and road surfaces as the attenuation level is too high [21]. Finally, for the windshield antenna location, there is a possibility to communicate through the front and rear windshields (W). We use ζ for the propagation path types, i.e., $\zeta \in \{L,U,R,W\}$.

The maximum communication distance for a hop that utilizes the propagation path through the windshield is given by

$$d_W(S) = \left(\frac{P_T \sqrt[10]{10^{G_A+G_U}}}{\sqrt[10]{10^{N_0+S}} 10^{2log_{10} f_c - 12,86}} \right)^{\frac{1}{\gamma}}, \quad (7)$$

while for side reflections available for all three considered antenna locations it takes the following form

$$d_R(S) = \left(\frac{P_T \sqrt[10]{10^{G_A+G_U}}}{\sqrt[10]{10^{N_0+S}} 10^{2log_{10} f_c - 14,36}} \right)^{\frac{1}{\gamma}}. \quad (8)$$

The under-vehicle propagation distance can be obtained numerically by utilizing the following relation

$$P_{T_W} - S = 20\log_{10} d_U(S) + 20\log_{10} f_c - \\ - 147.55 + \phi d_U(S)^{-\Psi}, \quad (9)$$

where P_{T_W} is the transmit power, ϕ and Ψ are the constants that reflect the antenna deployment [21]. Note that setting the minimum required signal power at Rx $S = S_{\min}$ allows us to obtain the maximum communication distance for a single hop, hereafter denoted as d_ζ^{max}, $\zeta \in \{L,U,R,W\}$, where L means LoS path, W corresponds to the windshield, R stands for side reflection, and U denotes under-vehicle propagation.

In our model, the data rate is defined by the modulation and coding schemes (MCS) specified in IEEE 802.15.3d standard. That is, once the communication distance falls into a range limited by received signal power, the corresponding data rate is shown in Table III. Further, Fig. 2 presents the data rates depending on communication distances for different scenarios of antenna deployment computed with available MCSs. Observe that for all the MCSs the communication distances follow the same strict order determined by the signal power from the highest to the lowest: LoS, under-vehicle, side reflection, and windshield. This provides us with natural priorities among the propagation paths which will be used further.

Recall that L_B depends on the considered communications scenario and can represent either blockage losses induced by propagation through the windshields or attenuation caused by reflections off the road surface or vehicle body. The attenuation levels of these impairments, as well as maximum communications distances, are summarized in Table IV.

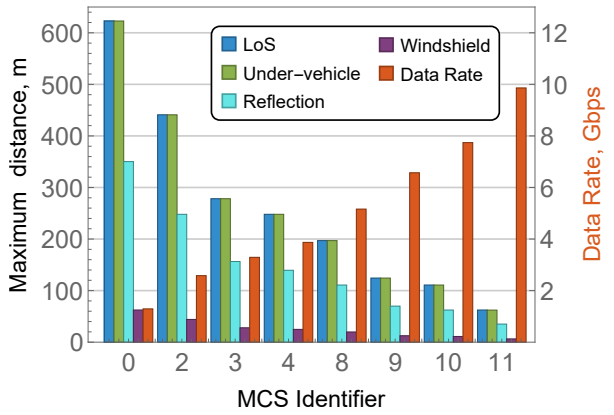

Fig. 2: Single hop communication distance and data rate.

B. Multi-Hop Characterization

Recall, that the probability density functions (pdf) of the distances [44] to the i-th neighbor in the Poisson process of vehicles follow Erlang distribution in the following form [45]

$$f_i(x) = \frac{2(\pi\lambda)^i}{(i-1)!} x^{2i-1} e^{-\pi\lambda x^2}, \; x > 0, \; i = 1,\ldots,N. \quad (10)$$

The random distances to the first and second nearest neighbors can be obtained by conditioning on the minimum separation distance between vehicles. These distances between the centers of the vehicles are given by $d_s = t_s v + l_v$ which leads to

$$f_1(s) = 2\lambda e^{-2\lambda(s-d_s)}, \\ f_2(s) = 4\lambda^2 (s-d_s) e^{-2\lambda(s-d_s)}, \quad (11)$$

where $f_1(s) = f_2(s) = 0$ when $s < d_s$.

1) Direct LoS Communications: To proceed further, denote the length of a single hop as r, and the distance between Tx antenna and blocker as d_O. Observe that LoS communications are always feasible in all the considered antenna locations as long as the distance between communicating vehicles is smaller than the maximum communication distance in LoS conditions, $d^{\max}$, available from (6), and the next vehicle is equipped with a communications system. This leads to the following probability of a successful direct hop in LoS conditions at the distance r

$$f_{H,LoS}(r) = I(r < d^{\max}) P_E f_O(r), \quad (12)$$

where the unknown term $f_O(r)$ given by

$$f_O(r) = 0.5 f_1(r) + 0.5 f_2(r). \quad (13)$$

TABLE IV: Additional losses over considered paths, L_B

Path	Max distance (m)	Losses (dB)
LoS	622.789	0
Under-Vehicle	622.788	1–27
Reflection	350.22	5
Windshield	62.278	20

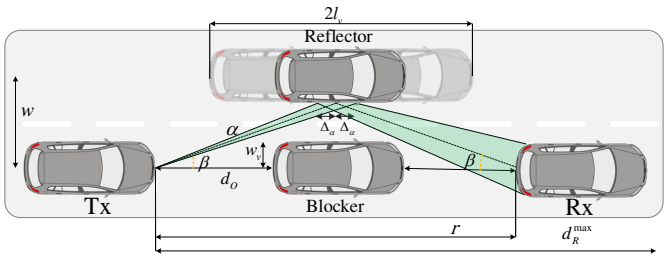

Fig. 3: Illustration of side reflection propagation path.

is the pdf of the distance to the next vehicle on the same lane which is the first or the second neighbour and $I(\cdot)$ is the indicator function.

2) Side-Reflection: Recall that side reflection is available for all the considered antenna locations. In the blockage scenario that is, when the next vehicle is not equipped with a communications system we assume that the distance to the blocking vehicle, d_O, is equiprobable and described by a mixture of the pdfs in (11) as in (13). By focusing on the blocking vehicle, the pdf of the distance to bypass a blocker is given by the convolution of the distances to the two nearest blocker-vehicle neighbors, i.e.,

$$f_B(r) = (f_1 * f_2)(r) = \int_0^{\infty} f_1(s) f_2(r-s) ds. \tag{14}$$

In our model, we assume that bypassing at most one vehicle is feasible. This stems from previous studies performed in the field [21], [24], [25]. In [25] it has been demonstrated that the probability of having a specific arrangement of the vehicles such that reflections of order higher than one are available at the target vehicle is rather small (in fact, the probability of having a reflection of order n decreases geometrically fast to zero). The under-vehicle propagation is geometrically limited to a single hop as the peculiar reflection having the strongest received power does not exist anymore for more than a single hop bypassing scenario. Finally, accounting for much higher losses at the considered frequency (300 GHz) as compared to other studies assessing mostly mmWave propagation (28/72 GHz), penetration losses of the windshield propagation are much higher (40 dB reported in [21] for a single vehicle, see Table IV) such no more than a single hop can be bypassed. Note that this assumption is in line with the results of [24].

Observe that the side reflection is only possible when there is a vehicle on the adjacent lane in a proper position, see Fig. 3. However, even if the reflector is at the right position, the propagation path can be still blocked when the blocker vehicle is too close to the communicating vehicles. The probability of non-blocked side reflection can be found as

$$\delta_R(r) = \frac{w_v}{\eta(r)} = \frac{w_v r}{2(w-w_v)}, \tag{15}$$

where $\eta(r) = 2(w-w_v)/r$ is the tangent of the beam deflection angle β, w_v is the vehicle half-width.

The probability to have a reflecting vehicle at the needed point, $P_R(r)$, can be obtained by utilizing the independence property of the Poisson process. We assume that any point of a vehicle's side may produce a feasible reflection. Besides, it is possible to beamform the antenna arrays in a way that the Tx and Rx beams are still aligned, which gives us an additional shift of $2\Delta_\alpha(r)$, see Fig. 3. Thus, based on the property of the Poisson process consisting in that a random point is uniformly distributed over the inter-vehicle distance [46], the sought probability is provided by

$$P_R(r) = \begin{cases} \left(\frac{N_l}{2}-1\right) \frac{\delta_R(r)\lambda}{[l_V+2\Delta_\alpha(r)]^{-1}}, & 2d_S < r < d_R^{\max}, \\ 0, & \text{otherwise}, \end{cases} \tag{16}$$

where Δ_α is the possible reflector shift, that still allows having a reflection, derived as

$$\Delta_\alpha(r) = \frac{r}{2} - \frac{\eta(r) r (1-\eta(r)\tan(\alpha/2))}{2(\eta(r)+\tan(\alpha/2))}. \tag{17}$$

Besides the side reflection, it is also possible to bypass a blocking vehicle by using other types of propagation paths. In the case of engine-level antenna deployment, the only bypass option is side reflection as both under- and through-vehicle propagation paths are completely blocked, i.e., the probability of bypassing, in this case, is $P_{B,E}(r) = 0$.

3) Under-Vehicle Propagation: In contrast to the windshield- and engine-level antenna deployments, with bumper-level deployment under-vehicle propagation, becomes feasible. However, if the blocker vehicle is too close to Rx or Tx, the path is still blocked as the proper road reflection does not exist. Due to the symmetric property of the reflected path, see Fig. 4, the minimum distance between the blocker and antenna on both sides is the same and given by

$$\delta_U(r) = \frac{r}{2}\left(1 - \frac{h_C}{h_A}\right) - \Delta_\alpha, \tag{18}$$

where h_C is the road clearance, h_A is the antenna height, Δ_α is the shift allowed for the HPBW obtained similarly to (17).

Then, recalling the property of the Poisson process consisting in that the points on an interval of a fixed length are distributed uniformly [46], the probability of under-vehicle propagation can be derived as

$$P_{B,B}(r) = \begin{cases} \delta_U(r)\left(\frac{h_C}{h_A} + \frac{\Delta_\alpha}{r}\right), 2d_S < r < d_U^{\max}, \\ 0, \text{otherwise}. \end{cases} \tag{19}$$

4) Propagation Through Windshield: Finally, we note that in the case of windshield-level antenna location, it is possible to establish a communication path through the front and rear vehicle glasses, but with rather higher losses, see Table IV, i.e., implying that

$$P_{B,W}(r) = \begin{cases} 1, & 2d_S < r < d_W^{max}, \\ 0, & \text{otherwise}. \end{cases} \tag{20}$$

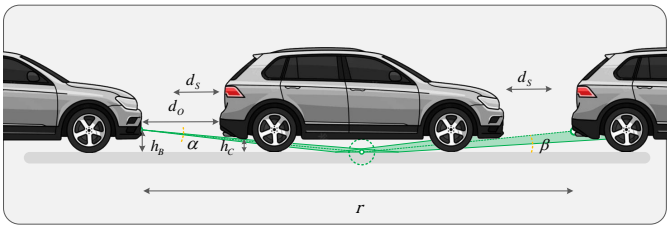

Fig. 4: Illustration of under-vehicle propagation.

TABLE V: Path usage probabilities

Path, ζ\Depl., σ	Bumper	Engine	Windshield
LoS	$1-P_O(r)$	$1-P_O(r)$	$1-P_O(r)$
Under-vehicle	$P_O(r)P_{B,B}(r)$	0	0
Reflection	$P_O(r)(1-P_{B,B}(r))$	$P_O(r)$	$P_O(r)P_R(r)$
Windshield	0	0	$P_O(r)(1-P_R(r))$

5) Multi-Hop Path Probability: Summarizing the abovementioned considerations, the probability of successful single-hop communications at the distance r, $f_{H,\sigma}(r)$, $\sigma \in \{B,E,W\}$, is defined as the sum of the two events: (i) either the next vehicle is equipped with an antenna and it is possible to utilize the direct LoS transmission, or (ii) next vehicle on the lane acts as a blocker with the probability $1-P_E$ and the only option is to bypass it. Thus, extending (12) with the probability of bypassing, we arrive at

$$f_{H,\sigma}(r) = I\left(r < d^{max}\right) P_E f_O(r) + \left(P_E - P_E^2\right) \times \\ \times \left(P_R(r) + P_{B,\sigma}(r) - P_R(r) P_{B,\sigma}(r)\right) f_B(r), \quad (21)$$

where $I(\cdot)$ is the indicator function.

C. Metrics of Interest

Having defined $f_{H,\sigma}(r)$ in (21), we are now in the position to proceed with the metrics of interest. Specifically, the probability that the bridge of n hops cover the distance r can be obtained using the n-power convolution of (21), that is,

$$p_{C,\sigma}(n,r) = \int_{r-d^{max}}^{\infty} f_{H,\sigma}^{(n)}(y)dy. \quad (22)$$

If we assume an infinite number of hops in a bridge, the probability of that the distance r is covered by the bridge can be derived as follows

$$p_S(r) = \sum_{i=1}^{\infty} p_{C,\sigma}(i,r) \prod_{j=1}^{i-1} (1 - p_{C,\sigma}(j,r)). \quad (23)$$

The data rate of a bridge [47] is defined by the hop with the worst channel conditions. Then, having the threshold values s_i, $i = 1,\ldots,N_C$, of Rx sensitivity corresponding to a set of channel quality indicators (CQI) $\{1,\ldots,N_C\}$ (see Table III) one may find the probability of using MCS i in a hop of type $\zeta \in \{L,U,R,W\}$ in the form

$$q_{\zeta,i} = \int_{d_\zeta(s_i)}^{d_\zeta(s_{i+1})} f_{H,\zeta}(r)\, dr, \; i = 1,\ldots,N_C, \quad (24)$$

where $d_\zeta(s_{N_C+1}) = \infty$.

Denote the probability of finding the next vehicle at the distance r by $P_O(r) = \int_0^r f_O(s)ds$. Then, the probability of using LoS path is defined by the condition of not finding any vehicle up to r, i.e.,

$$P_{L,\sigma} = \int_0^{\infty} (1 - P_O(s))\, f_O(s)ds. \quad (25)$$

TABLE VI: Road traffic parameters

Scenario	Jam	Normal	Highway
Vehicles speed, km/h	20	60	120
Inter-vehicle distance, m	10	30	60

The probabilities of using other paths depend on the priorities and follow the logic described below:

- For bumper antenna location ($\sigma = B$) the under-vehicle path depends on the path feasibility, defined as

$$P_{U,B} = \int_0^{\infty} P_O(s) P_{B,B}(s) f_O(s) ds. \quad (26)$$

  If it is not feasible, the side reflection is used instead with the following probability

$$P_{R,B} = \int_0^{\infty} P_O(s)(1 - P_{B,B}(s)) f_O(s) ds. \quad (27)$$

- For the windshield antenna deployment ($\sigma = W$), the side reflection is of priority, i.e.,

$$P_{R,W} = \int_0^{\infty} P_O(s) P_R(s) f_O(s) ds. \quad (28)$$

  If it is not feasible, the windshield path is used instead with probability

$$P_{W,W} = \int_0^{\infty} P_O(s)(1 - P_R(s)) f_O(s) ds. \quad (29)$$

- Finally, for engine level antenna location ($\sigma = E$), the side reflection is the only bypass option occurring with the probability

$$P_{R,E} = \int_0^{\infty} P_O(s) f_O(s) ds. \quad (30)$$

Summarizing the abovementioned probabilities, a certain path is utilized at a certain distance for each of the antenna deployment options taking into account their priorities as shown in Table V.

To derive the mean bridge rate we divide the communication period into intervals of two types: (i) active communication period and (ii) outage period caused by link unavailability. During active communication, the achievable rate is defined by the relaying link having the least rate in the bridge. By employing the binomial distribution with n trials, this rate is provided by

$$\rho_{\sigma,n} = \sum_{i=1}^{N_C} \omega_i \left(\sum_{\zeta \in \{L,U,R,W\}} P_{\zeta,\sigma} \sum_{k=i}^{N_C} q_{\zeta,k} \right)^n, \quad (31)$$

where ω_i is the spectral efficiency corresponding to the MCS i. In outage conditions, the data rate is simply zero. Accordingly, (23) allows us to find the share of time when active communication is feasible. Thus, the mean bridge rate is given by

$$\rho_{S,\sigma}(r) = \sum_{i=1}^{N} \rho_{\sigma,i} p_{C,\sigma}(i,r) \prod_{j=1}^{i} (1 - p_{C,\sigma}(j,r)). \quad (32)$$

Note that in (32) we limited the number of hops in a bridge to N. Recall that the main disadvantage of multi-hop V2X communications is the increased latency [48]. Even for underloaded traffic conditions, the packets' processing latency still increases linearly with the number of relays which may be inapplicable for various applications like video streaming, mission-critical applications, etc. Besides, the large number of hops complicates the bridge management in terms of signaling overhead and reduces bridge reliability. This induces an implicit constraint on the number of hops. Therefore, it has

TABLE VII: The default system parameters

Notation	Value	Description
l_v	4.5 m	Vehicle length
t_r	0.5 s	Minimal inter-vehicle distance
λ	0.02 un./m	Mean vehicle density
H_T	$0.4, 0.7, 1.2$ m	Antenna heights
H_V	0.2 m	Vehicle clearance
v	25 m/s	Default vehicle speed
f_c	304.2 GHz	Carried frequency [21]
P_T	$4.2 \cdot 10^{-6}$ W	BS/vehicle antenna emitted power [43]
P_{T_W}	-23.7 dBm	Emitted power [43]
N_0	-84 dBm	Noise power [43]
S	-56 dBm	Minimal SINR [43]
G_A, G_U	17.58 dBi	Transmit and receive side gains [43]
γ	2.1	Path loss exponent [21]
ϕ	23000	Propagation coefficient at 0.4 m [21]
ψ	3.4	Propagation coefficient at 0.4 m [21]

motivated us to include this constraint providing an opportunity to analyze the implicit trade-off between the latency and the coverage enhancement and bridge rate.

V. Numerical Results

In this section, we elaborate on our numerical results. We start with characterizing the trade-off between the mean bridge length and the mean data rate for different antenna locations. Then, we proceed with the maximum ISD in different environmental conditions and antenna locations. Further, we characterize the usage of different propagation paths for considered antenna locations. Finally, we compare the required BS density with and without relaying capabilities.

We consider four road traffic conditions: (i) traffic jam, (ii) normal traffic conditions, (iii) highway. These cases differ in the speed of the vehicles and the distance between them, as shown in Table VI. The rest of the system parameters are provided in Table VII. Note that whenever possible, we utilize practical values from IEEE 802.15.3d standard. On top of this, the propagation constants and specifics are taken from the measurement campaign carried out in [21] and summarized in Table I. Finally, the CQI to MCS mappings also follow IEEE 802.15.3d and are provided in Table III.

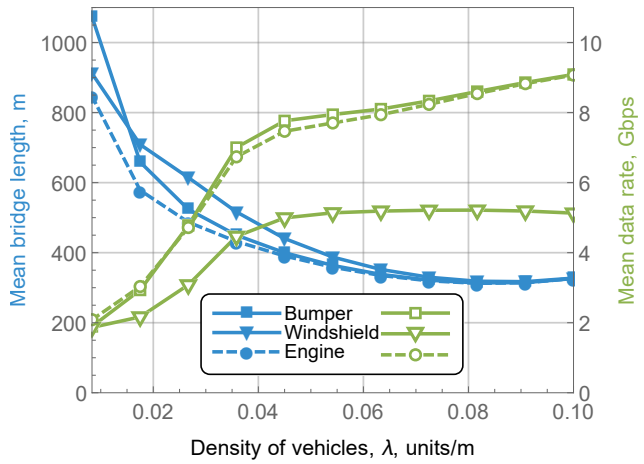

Fig. 5: Trade-off between the bridge length and data rate.

A. Main Trade-Offs and Dependencies

We start with investigating the basic trade-offs and dependencies between the mean bridge length and the data rate illustrated in Fig. 5 for different antenna locations as a function of the vehicle density, where the maximum number of hops is set to 10, and the technology penetration rate is $P_E = 0.7$. First of all, we observe that the mean bridge length decreases as the density of vehicles increases for all the considered antenna locations. This is explained by the fact that the mean distance between vehicles decreases with the increased vehicle density. The reverse effect is observed for the data rate and this is due to shorter inter-vehicle distances.

Note that the qualitative behavior of the bridge length and data rate metrics is similar for all the considered antenna locations. Here, the mean bridge length decreases monotonously with the increased density of vehicles. Conversely, there is a steep increase in the data rate as the density of vehicles changes from 0.02 veh./m to 0.04 veh./m (from 50 m to 25 m between vehicles). This is explained by the specifics of the utilized MCS reported in Table III. Specifically, in this range of distances, the spectral efficiency drastically increases.

Analyzing the impact of antenna locations, we observe that the windshield location provides higher distances for almost all the considered vehicles' densities. However, this gain comes at the expense of a much smaller data rate. Specifically, the gap between the windshield and other locations in terms of the data rate increases as the vehicle density increases and reaches 2 Gbps for 0.04 veh./m (25 m between vehicles) and then further to 4 Gbps for 0.1 veh./m (10 m between vehicles). The rationale is that there are high path losses when operating through the rear and front windows. Further, notice that there is almost no difference between bumper and engine antenna locations in terms of both metrics. The reason is that both these locations are characterized by almost similar dominating propagation paths, see Section V-C.

B. Bridge Availability

Note that the mean performance metrics reported in the previous section cannot be utilized to dimension cellular systems. The rationale is that the commercial deployments need to deliver performance guarantees to the users. For this reason, in this section, we study a distributional characteristic of the considered system – bridge availability.

We start with the bridge availability as a function of ISD shown in Fig. 6 for different technology penetration rates, 10 hops, and normal traffic conditions ($\lambda = 1/30$). First of all, notice that up until the ISD of 1250 m there is coverage provided by BSs. At this value, we observe a sharp drop that characterizes the distance where the bridge starts to operate. Note that further, the bridge availability remains intact for all the considered antenna locations up until approximately ISD of 1600 m implying that the ISD is extended by approximately 50%. Out of all the considered locations, the windshield one shows the best availability of 0.95 for the technology penetration rate of 0.9. Furthermore, this location is also much less sensitive to the technology penetration rate as it decreases

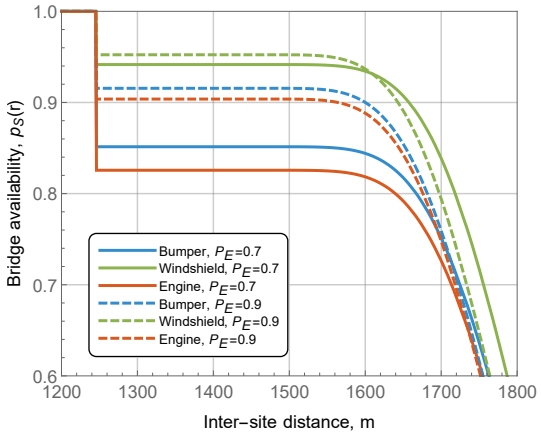

Fig. 6: Bridge availability as a function of ISD.

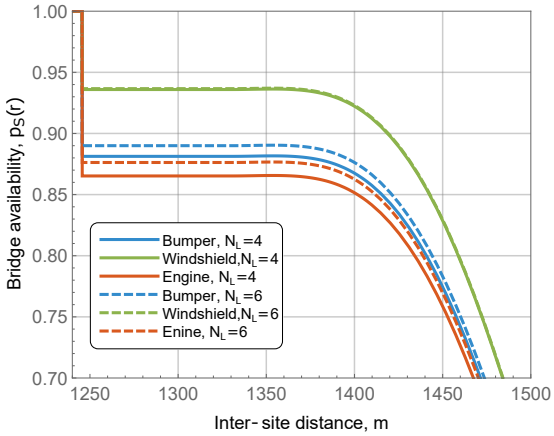

Fig. 8: Bridge availability as a function the number of lanes.

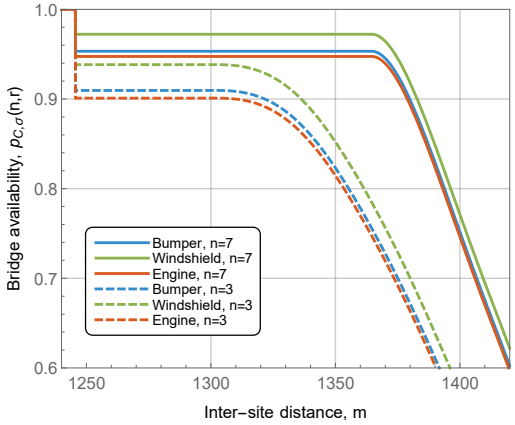

Fig. 7: Bridge availability for 3 and 7 hops.

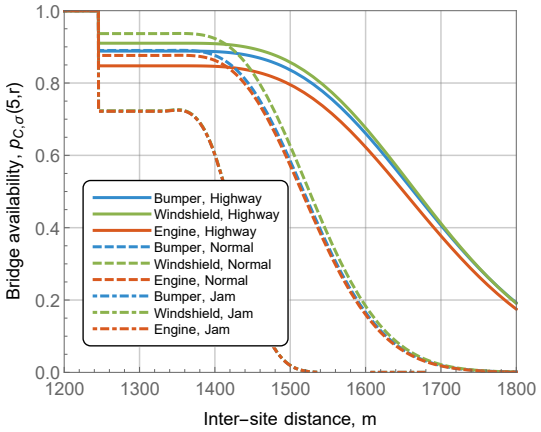

Fig. 9: Bridge availability as a function of traffic conditions.

by just $1-2\%$ for the penetration rate of 0.7 as compared to $10-15\%$ drop for other locations.

The impact of the number of hops on bridge availability is shown in Fig. 7 as a function of ISD for normal traffic conditions ($\lambda = 1/30$), and $P_E = 0.7$. Here, we observe that the number of hops produces a large impact on the ISD extension. Specifically, being limited by just 3 hops the coverage can only be extended by just 100 m which is around 10% while for the case of 7 hops – by 200 m which is approximately 16%. Thus, we may conclude that supporting many hops (e.g. > 10) is critical for the usage of relaying bridges.

The number of lanes is a characteristic feature of the roads. Highways are usually characterized by multiple lanes allowing to utilize reflections from both sides while there is only one reflection available on rural roads. In fact, the reflections can be utilized for all the considered antenna locations. To this aim, Fig. 8 shows the bridge availability as a function of ISD for one and two neighboring lanes for normal road traffic conditions ($\lambda = 1/30$), technology penetration rate $P_E = 0.7$, and the number of hops limited by 5. As one may observe, the number of lanes produces almost no impact on the bridge availability, especially, in the case of the windshield antenna location. The main reason is that the reflected paths are not heavily utilized as we will see in Section V-C.

Finally, we consider the impact of the road traffic conditions on the bridge availability in Fig. 9 for different antenna locations, where the maximum number of hops is set to 5. Here, we observe that the worst possible deployment is traffic jam conditions, where not only all the considered antenna locations result in the same ISD but the associated ISD improvement is insignificant (approximately 10%). The rationale is that vehicles are extremely densely positioned blocking multiple propagation paths including reflected and under-vehicle ones. As the road traffic conditions become sparser, the bridge length increases proportionally. Still, for normal and highway scenarios, the best antenna location in terms of the bridge length is the windshield.

C. Propagation Path Usage

We now proceed to discuss the use of the propagation paths for different antenna locations. To this aim, Fig. 10 shows the single-hop path usage probability as a function of the hop distance. Note that here we show bumper and windshield antenna locations only as the former one is characterized by similar results to engine location. By analyzing the presented data, we see that at small hop distances of up to 50 m, LoS propagation path dominates for both locations. Side reflections and even under-vehicle propagation are almost never utilized at these hop distances. As the hop distance increases, the use

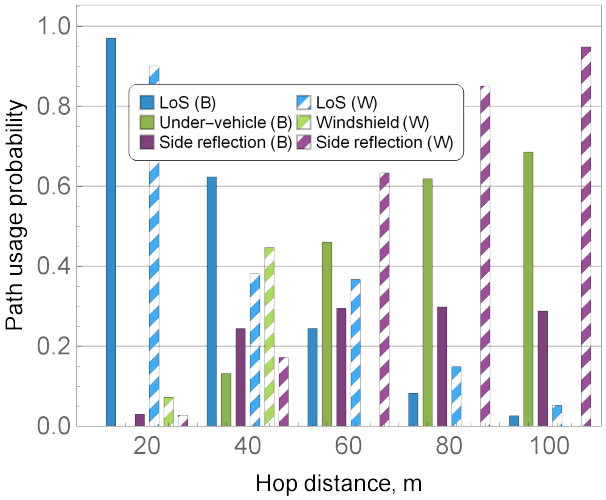

Fig. 10: Single hop path usage as a function of hop length.

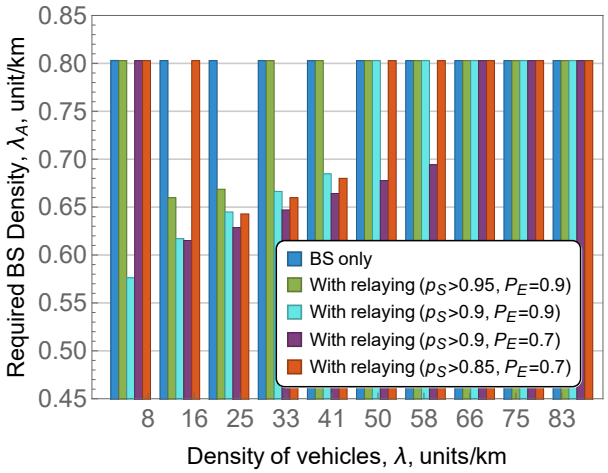

Fig. 11: The required BS density with and without relaying.

of the LoS path decreases while the latter two propagation paths start to be utilized more aggressively.

Two considered antenna locations differ at large hop distances. Here, in the case of windshield location reflections dominate as this is the only available path. However, for bumper level (and also engine level) location, under-vehicle propagation is heavily utilized along with reflections. The lack of this propagation path that is characterized by relatively good properties is the main reason for the much smaller data rate in the case of windshield antenna location reported in Fig. 5.

D. BS Density

We conclude our numerical exposure with the required BS density as a function of vehicles' density in Fig. 11 for different traffic conditions and technology penetration rate, 7 hops. Here, we also compare BS density with and without relaying functionality for different values of bridge availability, p_S. By analyzing the presented data, one may observe that by utilizing the relaying concept the required BS density is reduced up to 32% for $p_S > 0.9$ and $P_E = 0.9$ for sparse vehicles' density of approximately 8 units/km. As the density of vehicles increases, these gains gradually decrease reaching 10% for approximately 60 units/km. For other values of vehicles' density outside of the identified range, the gains are non-existence. Finally, we also note that the choice of p_S, P_E, and λ may have "binary" impact on the BS density, e.g., the gains for $p_S > 0.85$ and $P_E = 0.7$ is approximately 10% for $\lambda = 40$ units/km but immediately disappear already for $\lambda = 40$ units/km.

VI. Conclusion

In this paper, motivated by uncertainty with respect to optimal antenna locations on vehicles in future V2V communications, we developed a mathematical framework capable of characterizing the performance of multi-hop V2V communications operating in sub-THz frequency bands in different road traffic, system, and environmental conditions. The considered metrics of interest include mean bridge length and data rate as well as the critical quality of service parameter for network operator – bridge availability that allows assessing coverage extension provided by multi-hop communications.

The reported numerical results are based on IEEE 802.15.3d parameters and real measurements at 300 GHz. Specifically, we show that the qualitative behavior of the bridge length and data rate metrics are similar for all the considered antenna locations: for a fixed number of hops, bridge length decreases while the data rate increases. The windshield location is characterized by drastically lower data rates while bumper and engine levels are very similar in terms of mean bridge length and data rates. However, the former is less sensitive to the technology penetration rate and allows to provide bridge availability of 0.95 for up to 50% extended BS coverage. For all the considered locations, traffic jam conditions are characterized by the worst performance leading to just 10% extended BS coverage. However, as road traffic conditions become sparse the coverage linearly increases.

Based on the abovementioned conditions, the windshield location is recommended as in spite of the much lower data rate it is less sensitive to technology penetration rate and is generally characterized by the much larger coverage.

References

[1] D. Moltchanov, Y. Gaidamaka, D. Ostrikova, V. Beschastnyi, Y. Koucheryavy, and K. Samouylov, "Ergodic outage and capacity of terahertz systems under micromobility and blockage impairments," *IEEE Transactions on Wireless Communications*, pp. 1–16, 2021.

[2] D. Moltchanov, V. Beschastnyi, D. Ostrikova, Y. Gaidamaka, and Y. Koucheryavy, "Uninterrupted connectivity time in THz systems under user micromobility and blockage," in *2021 IEEE Global Communications Conference (GLOBECOM)*, pp. 01–06, IEEE, 2021.

[3] G. R. MacCartney, S. Deng, S. Sun, and T. S. Rappaport, "Millimeter-wave human blockage at 73 GHz with a simple double knife-edge diffraction model and extension for directional antennas," in *2016 IEEE 84th Vehicular Technology Conference (VTC-Fall)*, pp. 1–6, IEEE, 2016.

[4] M. Gapeyenko, A. Samuylov, M. Gerasimenko, D. Moltchanov, S. Singh, M. R. Akdeniz, E. Aryafar, N. Himayat, S. Andreev, and Y. Koucheryavy, "On the temporal effects of mobile blockers in urban millimeter-wave cellular scenarios," *IEEE Transactions on Vehicular Technology*, available online, 2017.

[5] N. V. Stepanov, D. Moltchanov, V. Begishev, A. Turlikov, and Y. Koucheryavy, "Statistical analysis and modeling of user micromobility for THz cellular communications," *IEEE Transactions on Vehicular Technology*, 2021.

[6] V. Petrov, D. Moltchanov, Y. Koucheryavy, and J. M. Jornet, "Capacity and outage of terahertz communications with user micro-mobility and beam misalignment," *IEEE Transactions on Vehicular Technology*, 2020.

[7] V. Beschastnyi, D. Ostrikova, D. Moltchanov, Y. Gaidamaka, Y. Koucheryavy, and K. Samouylov, "Balancing latency and energy efficiency in mmWave 5G NR systems with multiconnectivity," *IEEE Communications Letters*, pp. 1–5, 2022.

[8] ITU-R, "Minimum requirements related to technical performance for IMT-2020 radio interface," M.2410-0, ITU-R, July 2017.

[9] V. Petrov, D. Moltchanov, S. Andreev, and R. W. Heath, "Analysis of intelligent vehicular relaying in urban 5G+ millimeter-wave cellular deployments," in *2019 IEEE Global Communications Conference (GLOBECOM)*, pp. 1–6, IEEE, 2019.

[10] 3GPP, "Study on integrated access and backhaul (Release 17)," TR 38.874 V17.0.0, 3GPP, Dec. 2020.

[11] Y. Sadovaya, D. Moltchanov, W. Mao, O. Orhan, S.-p. Yeh, H. Nikopour, S. Talwar, and S. Andreev, "Integrated access and backhaul in millimeter-wave cellular: Benefits and challenges," *IEEE Communications Magazine*, 2022.

[12] 3GPP, "Study on architecture enhancements for 3GPP support of advanced Vehicle-to-Everything (V2X) services; Phase 2 (Release 17)," TR 23.776 V16.0.3, 3GPP, December 2020.

[13] M. Harounabadi, D. M. Soleymani, S. Bhadauria, M. Leyh, and E. Roth-Mandutz, "V2X in 3GPP standardization: NR sidelink in release-16 and beyond," *IEEE Communications Standards Magazine*, vol. 5, no. 1, pp. 12–21, 2021.

[14] A. Yamamoto, K. Ogawa, T. Horimatsu, A. Kato, and M. Fujise, "Path-loss prediction models for intervehicle communication at 60 GHz," *IEEE Transactions on vehicular technology*, vol. 57, no. 1, pp. 65–78, 2008.

[15] M. Boban, D. Dupleich, N. Iqbal, J. Luo, C. Schneider, R. Müller, Z. Yu, D. Steer, T. Jämsä, J. Li, *et al.*, "Multi-band vehicle-to-vehicle channel characterization in the presence of vehicle blockage," *IEEE access*, vol. 7, pp. 9724–9735, 2019.

[16] J.-J. Park, J. Lee, K.-W. Kim, K.-C. Lee, and M.-D. Kim, "Vehicle antenna position dependent path loss for millimeter-wave V2V communication," in *2018 11th Global Symposium on Millimeter Waves (GSMM)*, pp. 1–3, IEEE, 2018.

[17] J.-J. Park, J. Lee, J. Liang, K.-W. Kim, K.-c. Lee, and M.-D. Kim, "Millimeter wave vehicular blockage characteristics based on 28 GHz measurements," in *2017 IEEE 86th Vehicular Technology Conference (VTC-Fall)*, pp. 1–5, IEEE, 2017.

[18] S. Takahashi, A. Kato, K. Sato, and M. Fujise, "Distance dependence of path loss for millimeter wave inter-vehicle communications," in *2003 IEEE 58th Vehicular Technology Conference. VTC 2003-Fall (IEEE Cat. No. 03CH37484)*, vol. 1, pp. 26–30, IEEE, 2003.

[19] 3GPP, "Study on channel model for frequencies from 0.5 to 100 GHz (Release 14)," 3GPP TR 38.901 V14.1.1, 3GPP, July 2017.

[20] H. Wang, X. Yin, X. Cai, H. Wang, Z. Yu, and J. Lee, "Fading characterization of 73 GHz millimeter-wave V2V channel based on real measurements," in *International Workshop on Communication Technologies for Vehicles*, pp. 159–168, Springer, 2018.

[21] J. M. Eckhardt, V. Petrov, D. Moltchanov, Y. Koucheryavy, and T. Kürner, "Channel measurements and modeling for low-terahertz band vehicular communications," *IEEE Journal on Selected Areas in Communications*, vol. 39, no. 6, pp. 1590–1603, 2021.

[22] R. He, C. Schneider, B. Ai, G. Wang, Z. Zhong, D. A. Dupleich, R. S. Thomae, M. Boban, J. Luo, and Y. Zhang, "Propagation channels of 5G millimeter-wave vehicle-to-vehicle communications: Recent advances and future challenges," *IEEE vehicular technology magazine*, vol. 15, no. 1, pp. 16–26, 2019.

[23] V. Petrov, J. M. Eckhardt, D. Moltchanov, Y. Koucheryavy, and T. Kurner, "Measurements of reflection and penetration losses in low terahertz band vehicular communications," in *2020 14th European Conference on Antennas and Propagation (EuCAP)*, pp. 1–5, IEEE, 2020.

[24] M. Ozpolat, K. Bhargava, E. Kampert, and M. D. Higgins, "Multi-lane urban mmwave V2V networks: A path loss behaviour dependent coverage analysis," *Vehicular Communications*, vol. 30, p. 100348, 2021.

[25] V. Petrov, J. Kokkoniemi, D. Moltchanov, J. Lehtomäki, M. Juntti, and Y. Koucheryavy, "The impact of interference from the side lanes on mmWave/THz band V2V communication systems with directional antennas," *IEEE Transactions on Vehicular Technology*, vol. 67, no. 6, pp. 5028–5041, 2018.

[26] O. A. Saraereh, A. Ali, I. Khan, and K. Rabie, "Interference analysis for vehicle-to-vehicle communications at 28 GHz," *Electronics*, vol. 9, no. 2, 2020.

[27] Z. Li, L. Xiang, X. Ge, G. Mao, and H.-C. Chao, "Latency and reliability of mmWave multi-hop V2V communications under relay selections," *IEEE Transactions on Vehicular Technology*, vol. 69, no. 9, pp. 9807–9821, 2020.

[28] H. Hashemi, J. Haghighat, and M. Eslami, "Performance analysis of relay-aided millimeter-wave communications with optimal and sub-optimal combining at destination," *Physical Communication*, vol. 39, p. 100991, 2020.

[29] M. Hussain, M. Scalabrin, M. Rossi, and N. Michelusi, "Mobility and blockage-aware communications in millimeter-wave vehicular networks," *IEEE Transactions on Vehicular Technology*, vol. 69, no. 11, pp. 13072–13086, 2020.

[30] J. Wang, J. Liu, and N. Kato, "Networking and communications in autonomous driving: A survey," *IEEE Communications Surveys & Tutorials*, vol. 21, no. 2, pp. 1243–1274, 2018.

[31] P. Boronin, V. Petrov, D. Moltchanov, Y. Koucheryavy, and J. M. Jornet, "Capacity and throughput analysis of nanoscale machine communication through transparency windows in the terahertz band," *Nano Communication Networks*, vol. 5, no. 3, pp. 72–82, 2014.

[32] J. M. Jornet and I. F. Akyildiz, "Channel modeling and capacity analysis for electromagnetic wireless nanonetworks in the terahertz band," *IEEE Transactions on Wireless Communications*, vol. 10, no. 10, pp. 3211–3221, 2011.

[33] L. S. Rothman *et al.*, "High-resolution transmission molecular absorption database," Harvard-Smithson Center for Astrophysics, www.cfa.harvard.edu, HITRAN, 2014.

[34] V. Petrov, M. Komarov, D. Moltchanov, J. M. Jornet, and Y. Koucheryavy, "Interference and SINR in millimeter wave and terahertz communication systems with blocking and directional antennas," *IEEE Transactions on Wireless Communications*, vol. 16, no. 3, pp. 1791–1808, 2017.

[35] S. Singh, R. Mudumbai, and U. Madhow, "Interference analysis for highly directional 60-GHz mesh networks: The case for rethinking medium access control," *IEEE/ACM Transactions on Networking*, vol. 19, no. 5, pp. 1513–1527, 2011.

[36] A. B. Constantine *et al.*, "Antenna theory: analysis and design," *Microstrip Antennas, John Wiley & Sons*, 2005.

[37] R. Kovalchukov, D. Moltchanov, A. Samuylov, A. Ometov, S. Andreev, Y. Koucheryavy, and K. Samouylov, "Analyzing effects of directionality and random heights in drone-based mmWave communication," *IEEE Transactions on Vehicular Technology*, vol. 67, no. 10, pp. 10064–10069, 2018.

[38] R. Kovalchukov, D. Moltchanov, A. Samuylov, A. Ometov, S. Andreev, Y. Koucheryavy, and K. Samouylov, "Evaluating SIR in 3D millimeter-wave deployments: Direct modeling and feasible approximations," *IEEE Transactions on Wireless Communications*, vol. 18, no. 2, pp. 879–896, 2019.

[39] M. Gerasimenko, D. Moltchanov, M. Gapeyenko, S. Andreev, and Y. Koucheryavy, "Capacity of multiconnectivity mmWave systems with dynamic blockage and directional antennas," *IEEE Transactions on Vehicular Technology*, vol. 68, no. 4, pp. 3534–3549, 2019.

[40] S. Henry, A. Alsohaily, and E. S. Sousa, "5g is real: Evaluating the compliance of the 3gpp 5g new radio system with the itu imt-2020 requirements," *IEEE Access*, vol. 8, pp. 42828–42840, 2020.

[41] J. T. Penttinen, "On 6g visions and requirements," *Journal of ICT Standardization*, pp. 311–326, 2021.

[42] M. Fuentes, J. L. Carcel, C. Dietrich, L. Yu, E. Garro, V. Pauli, F. I. Lazarakis, O. Grøndalen, O. Bulakci, J. Yu, *et al.*, "5g new radio evaluation against imt-2020 key performance indicators," *IEEE Access*, vol. 8, pp. 110880–110896, 2020.

[43] V. Petrov, T. Kurner, and I. Hosako, "IEEE 802.15. 3d: First standardization efforts for sub-terahertz band communications toward 6G," *IEEE Communications Magazine*, vol. 58, no. 11, pp. 28–33, 2020.

[44] D. Moltchanov, "Distance distributions in random networks," *Elsevier Ad Hoc Networks*, vol. 10, no. 6, pp. 1146–1166, 2012.

[45] G. Basharin, Y. V. Gaidamaka, and K. E. Samouylov, "Mathematical theory of teletraffic and its application to the analysis of multiservice communication of next generation networks," *Automatic Control and Computer Sciences*, vol. 47, no. 2, pp. 62–69, 2013.

[46] J. F. C. Kingman, *Poisson processes*. Wiley Online Library, 1993.

[47] V. Naumov, Y. Gaidamaka, N. Yarkina, and K. Samouylov, *Matrix and Analytical Methods for Performance Analysis of Telecommunication Systems*. Springer Nature Switzerland AG, 2021.

[48] K. Lee, J. Kim, Y. Park, H. Wang, and D. Hong, "Latency of cellular-based v2x: Perspectives on tti-proportional latency and tti-independent latency," *IEEE Access*, vol. 5, pp. 15800–15809, 2017.